Article

Preparation, Thermal, and Physical Properties of Perovskite-Type (C₃H₇NH₃)₂CdCl₄ Crystals

Ae Ran Lim [1,2,*] and Sun Ha Kim [3,4]

[1] Analytical Laboratory of Advanced Ferroelectric Crystals, Jeonju University, Jeonju 55069, Korea
[2] Department of Science Education, Jeonju University, Jeonju 55069, Korea
[3] Korea Basic Science Institute, Seoul Western Center, Seoul 120-140, Korea; sunha@kbsi.re.kr
[4] Department of Chemistry, Kyungpook National University, Daegu 41566, Korea
[*] Correspondence: aeranlim@hanmail.net

check for updates

Abstract: To investigate the thermal and physical properties of perovskite-type $(C_3H_7NH_3)_2CdCl_4$, its temperature-dependent chemical shifts and spin–lattice relaxation times are measured using thermogravimetric analysis (TGA), differential scanning calorimetry (DSC), magic angle spinning nuclear magnetic resonance (MAS NMR), and static NMR methods. Above 300 K, two phase transitions are observed at 398 K and 538 K. Each proton and carbon in the $(C_3H_7NH_3)$ cation is distinguished in the MAS NMR results. The environments around ^1H, ^{13}C, and ^{14}N do not change with temperature according to the NMR spectra. In contrast, the resonance frequency of ^{113}Cd in the $CdCl_6$ octahedra decreases with increasing temperature, indicating an environmental change. The uniaxial rotations for ^1H and ^{13}C have high mobility at both high and low temperatures, and these are related to the phase transitions. In addition, the molecular motion of ^{113}Cd in the anion becomes activated upon raising the temperature.

Keywords: perovskite; $(C_3H_7NH_3)_2CdCl_4$; NMR; phase transition

1. Introduction

Organic–metal hybrid compounds provide many opportunities for potential applications [1–6]. In these materials, a large number of organic and metal moieties with different properties can be combined within a single structure. Hybrid organic–metal compounds based on the perovskite structures were first reported in 1976, and recently there is increasing interest in them due to their potential as substitutes for perovskite [7,8]. Especially, layered perovskite-type compounds with the formula $(C_nH_{2n+1}NH_3)_2MX_4$ (M = divalent metal, X = halogen ion) have interesting physical properties [9–16]. These compounds consist of inorganic layers of corner-sharing MX_6 octahedra and organic layers of alkylammonium ions. N–H···X hydrogen bonds are formed between the NH_3^+ polar heads of the alkylammonium and the halogen atoms, and the polar heads occupy cavities among the octahedra [17]. In these materials, the cation dynamics and ion–ion interactions through hydrogen bonds affect the physical properties and thermal properties of structural phase transitions.

Previous studies have shown that the compound, when n = 3 and X = Cl, $(C_3H_7NH_3)_2CdCl_4$, undergoes three phase transitions below 300 K [16–18]. At 183 K, 156 K, and 105 K, they move from normal (N) to incommensurate (IC) to commensurate (C), and to another commensurate (C') phases respectively with the decreasing temperature. The N phase at room temperature has an orthorhombic structure, and its space group is *Abma* (Z = 4). In addition, at a higher temperature (535 K), a ferroelastic transition was reported to occur from the tetragonal phase (point group 4/*mmm*) to the ferroelastic orthorhombic phase (point group *mmm*) [19,20]. The lattice constants of the latter were a = 7.585 Å, b = 7.359 Å, and c = 25.053 Å [21,22]. The NH₃ polar head of the alkylammonium chain points toward

the layer of $CdCl_6$ to form hydrogen bonds with Cl^- in $CdCl_6$, while the alkyl chains point away from the $CdCl_6$ layer [23].

Using nuclear magnetic resonance (NMR) techniques, Blinc et al. [24] and Suzuki et al. [17] reported the spin–lattice relaxation times in the laboratory frame T_1 for ^1H and ^2H in $(C_3H_7NH_3)_2CdCl_4$ at low temperatures. However, the protons in C_3H_7 and NH_3 were not distinguished from each other. The structural phase transition at low temperature was reported to be connected with a change in the motion of the alkyl groups. The cation motion associated with the molecular axis was found to become activated at higher temperatures.

Solid state ^{13}C magic angle spinning (MAS) NMR, has proven to be a very powerful tool for studying the difference of the C–H vectors at different sites. The ^{13}C spin–lattice relaxation time in the rotating frame $T_{1\rho}$ is not influenced by spin diffusion due to the weak dipolar coupling, which results from the low natural abundance and large separation of the nuclei [25]. The $T_{1\rho}$ measured by MAS NMR allows a probing molecular motion in the kHz range, whereas that in the laboratory frame T_1 measured by static NMR reflects motion in the MHz range. Although the structural phase transitions of $(C_3H_7NH_3)_2CdCl_4$ at low temperature have been examined by a few research groups [17,24], the corresponding phenomena at high temperatures have not been fully studied.

Here, we discuss the organic–metal hybrid $(C_3H_7NH_3)_2CdCl_4$ crystal that was grown. The thermal and physical properties are discussed using thermogravimetric analysis (TGA), differential scanning calorimetry (DSC), and MAS NMR. The chemical shifts and $T_{1\rho}$ of $(C_3H_7NH_3)_2CdCl_4$ were measured using ^1H MAS NMR, ^{13}C cross-polarization (CP)/MAS NMR, and ^{14}N MAS NMR in order to clarify the structural geometry and dynamics of the cation. Each proton and carbon in the $(C_3H_7NH_3)$ cation was distinguished by MAS NMR. Additionally, the chemical shift and T_1 value for ^{113}Cd were obtained as a function of temperature. The dynamics of the cation and anion near the phase transition temperatures are discussed. In addition, the ferroelastic domain walls were observed by optical polarizing microscopy.

2. Experimental Section

Single crystals of $(C_3H_7NH_3)_2CdCl_4$ were grown by slowly evaporating an aqueous solution containing $C_3H_7NH_3Cl$ and $CdCl_2$ in 2:1 molar ratio at 27 °C. The obtained single crystals were transparent with a thin-plate shape. In addition, to determine the phase transition temperatures, DSC was carried out on the crystals with a Dupont 2010 DSC instrument under a heating rate of 10 K/min.

The NMR signals and the $T_{1\rho}$ values of $(C_3H_7NH_3)_2CdCl_4$ were obtained for powder materials by solid state ^1H MAS NMR, ^{13}C CP/MAS NMR, and ^{14}N MAS NMR at the respective Larmor frequencies of $\omega_0/2\pi$ = 400.13, 100.61, and 43.34 MHz. The instruments were the Bruker 400 MHz NMR and Unity INOVA 600 MHz NMR spectrometers at the Korea Basic Science Institute, Western Seoul Center. The chemical shifts were referenced to tetramethylsilane (TMS) and NH_4Cl. For all ^1H, ^{13}C, and ^{14}N measurements, the powder sample was loaded into a 4-mm CP/MAS probe, and the MAS rate was set to 10 kHz to minimize spinning sideband overlap. The ^1H $T_{1\rho}$ values were obtained using a $\pi/2-t$ sequence by varying the spin-locking pulse durations. The ^{13}C $T_{1\rho}$ values were obtained by changing the duration of the spin-locking pulse applied after the CP preparation period. The width of the $\pi/2$ pulse used for measuring $T_{1\rho}$ of ^1H and ^{13}C was 3.7 µs, and the spin-locking field was 67.56 kHz. The ^{14}N MAS NMR signals were recorded using a $\pi/2-t$ sequence, and the pulse width was 4 µs. The ^{113}Cd NMR spectra and the T_1 values of the single crystals were measured using a Bruker 400 MHz NMR spectrometer. The static magnetic field was 9.4 T, and the central radio frequency was set to $\omega_0/2\pi$ = 88.73 MHz. The T_1 value of ^{113}Cd was measured using saturation recovery pulse sequence $sat-t-\pi/2$. Nuclear magnetizations of ^{113}Cd nuclei at time t after the *sat* pulse were determined following the $\pi/2$ excitation pulse, and the $\pi/2$ pulse was 4.2 µs wide. The NMR spectra were recorded at temperatures of 180–430 K. Relaxation time outside this range could not be measured because of the limitations of the spectrometer used.

3. Results and Discussion

DSC analysis was used to determine phase transition temperatures of the $(C_3H_7NH_3)_2CdCl_4$ crystal. Three endothermic peaks related to phase transitions were observed at 178 K (T_{C3}), 398 K (T_{C2}), and 538 K (T_{C1}), as shown in Figure 1. Here, the transition temperatures of 178 K and 538 K are consistent with those reported by White et al. [26] and Ecolivet and Kusto [19], respectively. Meanwhile, the phase transition corresponding to the endothermic peak at 398 K has not been reported on before. On the other hand, DSC analysis at above 300 K was used to understand the temperature dependence. The curves reveal two endothermic peaks (T_{C2} and T_{C1}) during heating, and one exothermic peak (T_{C2}) during cooling, as shown in the inset of Figure 1. This change is irreversible with respect to temperature.
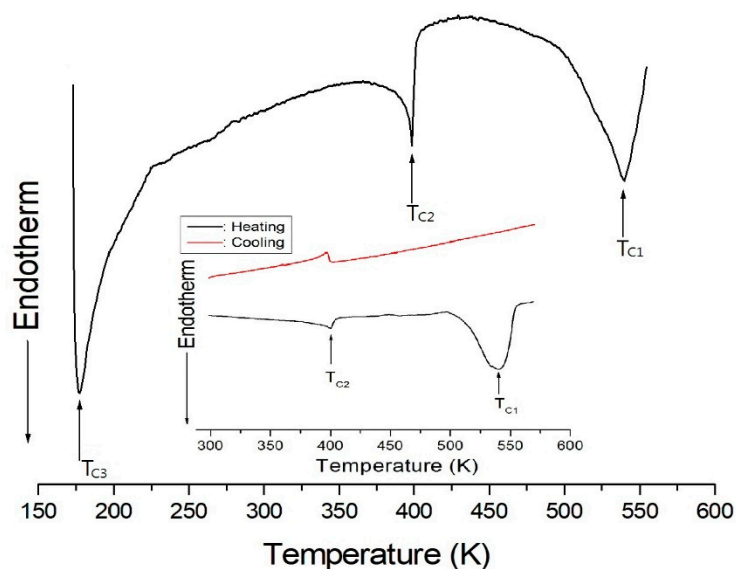

Figure 1. DSC thermogram of $(C_3H_7NH_3)_2CdCl_4$ crystal.

Figure 2 shows the TGA and DSC curves under a N_2 atmosphere above 300 K. Minor weight loss of 1% is observed in the TGA for $(C_3H_7NH_3)_2CdCl_4$ at a temperature as low as 398 K, which is ascribed to the onset of partial thermal decomposition. There is a sudden weight loss at 538 K and it is attributed to the beginning of $C_3H_7NH_2$ and HCl evaporations. The weight loss was sharp between 540 and 617 K, with a corresponding weight loss of 36.5%. The DSC study results were used to confirm the presence of structural transitions below the melting/decomposition temperature. In the DSC curve, the endothermic peak at 398 K corresponds to a phase transition, while the endothermic peaks at 561 and 576 K ($=T_d$) indicate the decomposition of $(C_3H_7NH_3)_2CdCl_4$. Optical polarizing microscopic images (Figure 2a–c) showed that the crystals were colorless and transparent at 293–473 K.
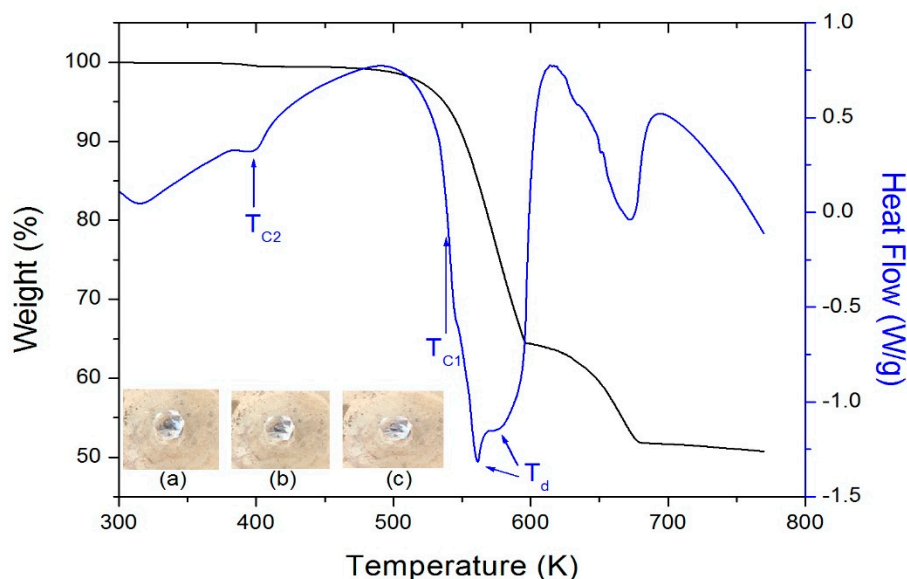
Figure 2. TGA and DSC curves of $(C_3H_7NH_3)_2CdCl_4$ crystals. Insets show color of the crystal at (**a**) 293 K, (**b**) 393 K, and (**c**) 473 K.

The ^1H NMR spectra were obtained by MAS NMR, and the spectrum at 300 K shows two peaks (inset in Figure 3). The spinning sidebands are denoted with crosses and asterisks. The spectrum consists of two distinct peaks at δ = 2.77 and 7.18 ppm, which are assigned to the ^1H in C_3H_7 and NH_3, respectively. Both of these peaks have nearly constant chemical shift upon increasing the temperature; therefore, the local structures of the different ^1H atoms remained similar.
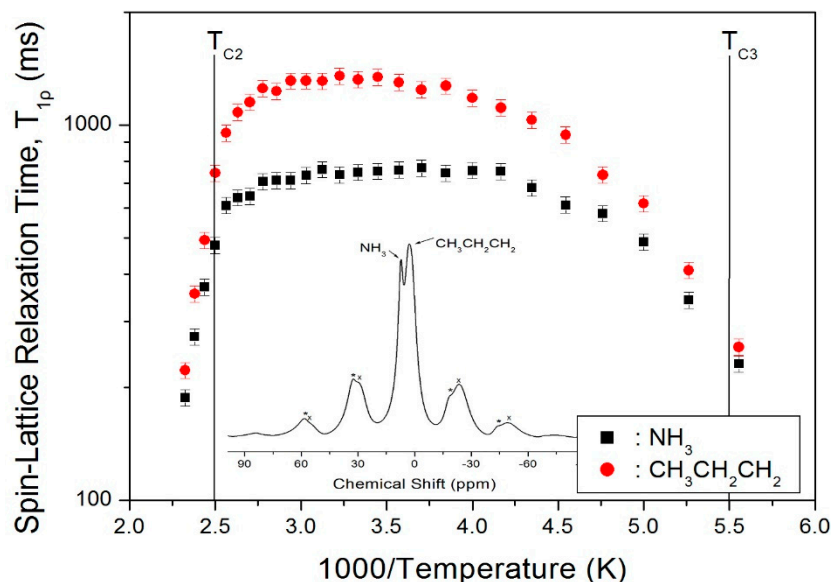
**Figure 3.** $T_{1\rho}$ values of ^1H in the C_3H_7 and NH_3 groups vs. 1000/T. Inset: ^1H MAS NMR spectrum of $(C_3H_7NH_3)_2CdCl_4$ at 300 K. The spinning sidebands are marked with crosses and asterisks.

The nuclear magnetization decay of ^1H is single exponential $S(t)/S_0 = \exp(-t/T_{1\rho})$, and the value of $T_{1\rho}$ can be determined by fitting the traces [25,27,28]. The recovery curves for various delay times were measured at given temperatures, and the recovery traces have different slopes. This way, we could obtain the $T_{1\rho}$ values for each proton in C_3H_7 and NH_3, and plot them vs. 1000/T in Figure 3. The ^1H $T_{1\rho}$ data all show similar trends with temperature, although the values are smaller for NH_3 than for C_3H_7. The $T_{1\rho}$ values abruptly decreases when the temperature approaches T_{C2} = 398 K,

and the values above T_{C2} were short at hundreds of ms. Additionally, when the temperature decreases to near 180 K (T_{C3}), $T_{1\rho}$ also becomes very short, like the case above 398 K, due to the impending phase transition. Therefore, although the local environments of ^{1}H suggested by the chemical shifts do not change with temperature, the molecular motion according to $T_{1\rho}$ is very active at both high and low temperatures.

The ^{13}C CP/MAS NMR spectrum of $(C_3H_7NH_3)_2CdCl_4$ at room temperature shows three peaks at 12.42, 21.46, and 43.41 ppm that are assignable to CH$_3$-3, CH$_2$-2, and CH$_2$-1, respectively, as shown in Figure 4. The crystal structure is confirmed from the chemical shifts obtained by the ^{13}C MAS NMR method, and it is also consistent with the report by Suzuki et al. [17]. The peak of CH$_3$-3 at 12.42 ppm is relatively stronger, and all three ^{13}C chemical shifts are temperature-independent. Therefore, the local environments of ^{13}C do not change with the temperature based on the chemical shifts of $(C_3H_7NH_3)$ cations. To obtain the ^{13}C $T_{1\rho}$ values, the nuclear magnetization is also measured as a function of delay time at several temperatures, and the ^{13}C NMR spectrum at 300 K is shown in the inset of Figure 5. The signal intensity in the ^{13}C nuclear magnetization recovery curves can be described by a single exponential function at all temperatures. For each carbon in $(C_3H_7NH_3)_2CdCl_4$, the calculated $T_{1\rho}$ values are plotted vs. 1000/T in Figure 5. The $T_{1\rho}$ values for CH$_3$-3, CH$_2$-2, and CH$_2$-1 all increase similarly with increasing temperature. At 398 K (T_{C2}), the spin–lattice relaxation time abruptly decreases with temperature like the case of ^{1}H $T_{1\rho}$, and this is related to the phase transition. On the other hand, the ^{13}C $T_{1\rho}$ values near T_{C3} are more or less continuous. The $T_{1\rho}$ values are 105.9, 38.5, and 40 ms for CH$_3$-3, CH$_2$-2, and CH$_2$-1 at 300 K, respectively. The much longer $T_{1\rho}$ of CH$_3$-3 is consistent with the fact that the dipolar relaxation is made more efficient when there are more bound protons. The side chains have additional mobility because of the internal rotation.
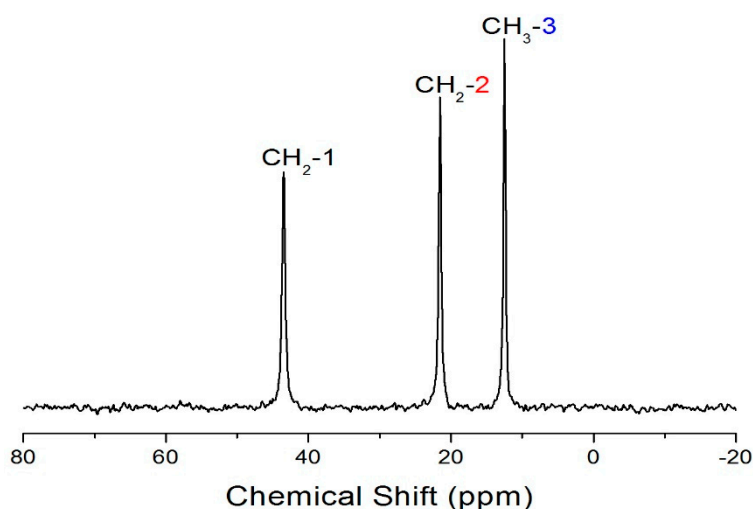

Figure 4. ^{13}C CP/MAS NMR spectrum of $(CH_3CH_2CH_2NH_3)_2CdCl_4$ at 300 K.
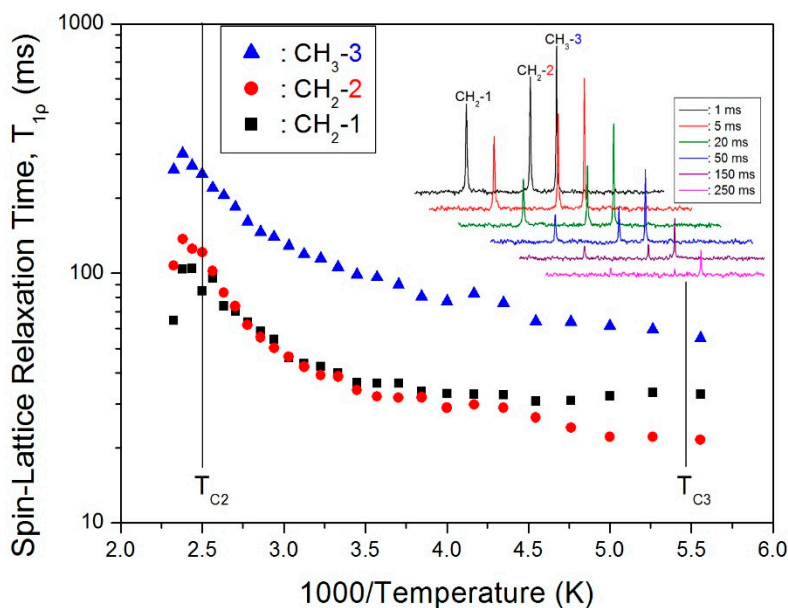
Figure 5. Spin–lattice relaxation times in the rotating frame $T_{1\rho}$ for each group of carbon in $(CH_3CH_2CH_2NH_3)_2CdCl_4$ vs. 1000/T. Inset: Recovery trace for each carbon at different delay times and 300 K.

Chemical shifts of ^{14}N in $(C_3H_7NH_3)_2CdCl_4$ were also studied using ^{14}N MAS NMR. The room-temperature spectrum shows one signal at δ = 6.71 ppm when referenced to NH_4Cl (inset in Figure 6). This signal shows no temperature dependence, indicating that the local environment surrounding ^{14}N in the NH_3^+ group hardly changes.
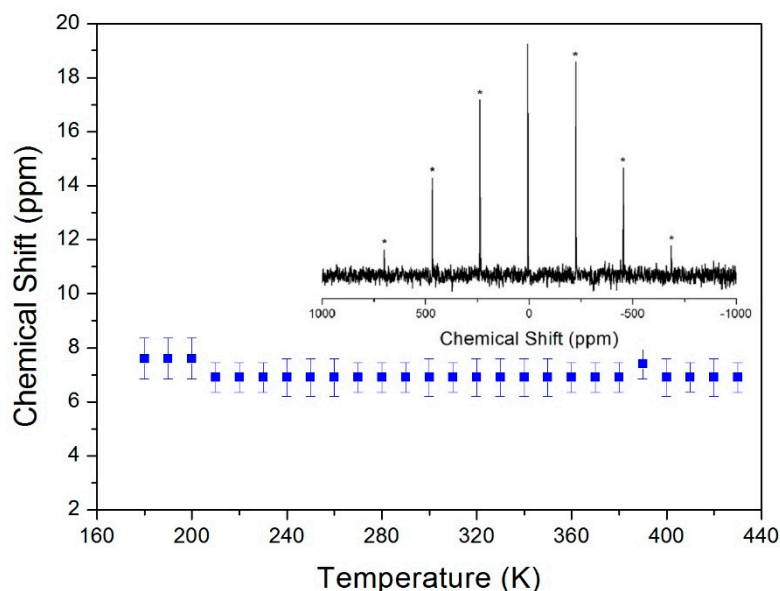
**Figure 6.** Chemical shift in ^{14}N MAS NMR spectra in $(C_3H_7NH_3)_2CdCl_4$ vs. temperature. Inset: Spectrum at 300 K, and the spinning sidebands are marked with asterisks.

^{113}Cd has a spin of I = 1/2 and its natural abundance is 12.3%. ^{113}Cd NMR experiments have been employed to examine the structure and dynamics of several organic and inorganic materials [29]. We did not perform the ^{113}Cd MAS NMR experiment because the ^{113}Cd NMR signals are well detected with single crystals despite the low natural abundance ratio. The ^{113}Cd static NMR spectrum consists of one peak at all temperatures. As shown in the inset of Figure 7, from 180 K to 420 K this resonance

frequency for [113]Cd signal decreases almost linearly. This result indicates that the environment of chloride surrounding the Cd is changed. The chemical shift of the Cd resonance lines is due to the contributions of the Cl ions [22]. The [113]Cd saturation recovery plots of $(C_3H_7NH_3)_2CdCl_4$ single crystals were obtained at several temperatures by using a static NMR method, and were fitted with a single exponential function $S(\infty)-S(t)/S(\infty)=\exp(-Wt)=\exp(-t/T_1)$ [30]. The T_1 value, given by $T_1=1/W$, decreases upon increasing the temperature, as shown in Figure 7. At low temperatures, T_1 is very long in the order of 1000 s, but shortened to approximately 400 s at high temperatures. This temperature dependence of T_1 follows a single Arrhenius relation, $T_1=T_0\exp(-E_a/RT)$, where T_0 is a pre-exponential factor, T is the temperature, R is the gas constant, and E_a is the activation energy. From the log T_1 vs. $1000/T$ plot, the E_a value for the molecular motion was found to be 3.64 ± 0.14 kJ/mol.
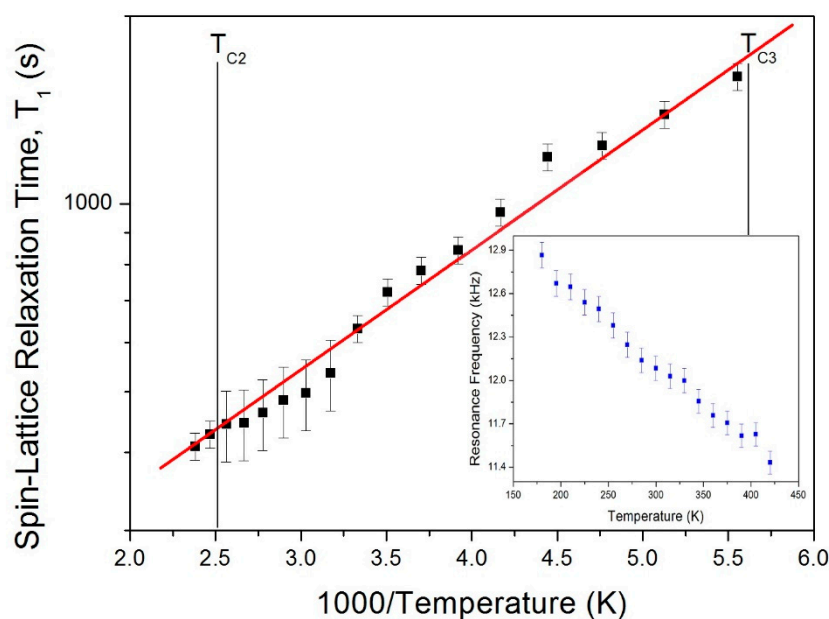
Figure 7. Spin–lattice relaxation times in the laboratory frame T_1 for [113]Cd in $(C_3H_7NH_3)_2CdCl_4$ crystals vs. $1000/T$. Inset: Resonance frequency of [113]Cd in $(C_3H_7NH_3)_2CdCl_4$ crystals at different temperatures.

A crystal is ferroelastic if (1) it has two or more stable orientation states in the absence of mechanical stress or an electric field and (2) transition between these orientation states can be induced by the application of mechanical stress [31]. Upon heating, the ferroelastic effect usually disappears at a well-defined temperature. The domain structures at several temperatures are observed by optical polarizing microscopy. Figure 8 shows the domain patterns at (a) 300 K, (b) 350 K, (c) 400 K, (d) 450 K, (e) 480 K, and (f) 500 K. The microscopic domain walls represented by parallel lines are due to the ferroelastic property [32]. A magnification of 200x was used to take pictures of the domain walls. The domain pattern at high temperature became dimmer and faded out. Additionally, ferroelastic domains exist in all ferroelastic crystals because of the reduction in symmetry between the paraelastic and ferroelastic phases [33,34]. To change from a tetragonal structure (point group 4/*mmm*) to an orthorhombic one (point group *mmm*), the domain wall orientations can be expressed as x = 0 and y = 0. These equations of twin boundaries indicate the ferroelasticity of the 4/*mmm*F*mmm* species, where 4/*mmm* is the symmetry above 538 K, *mmm* is the symmetry below 538 K, and F represents the ferroelastic phase.
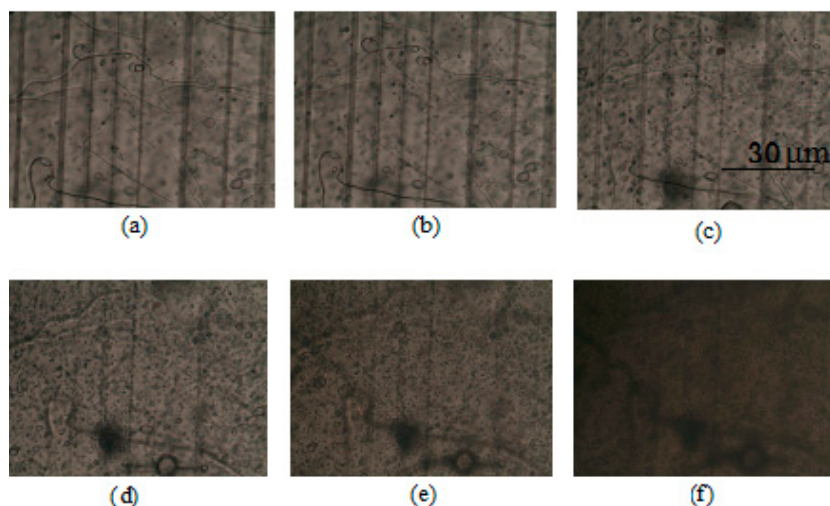
Figure 8. Optical polarizing microscopy images of $(C_3H_7NH_3)_2CdCl_4$ single crystals at (**a**) 300 K, (**b**) 350 K, (**c**) 400 K, (**d**) 450 K, (**e**) 480 K, and (**f**) 500 K. The ferroelastic domain walls are represented as parallel lines.

4. Conclusions

The thermal and physical properties of perovskite-type $(C_3H_7NH_3)_2CdCl_4$ were investigated by TGA, DSC, MAS NMR, and static NMR methods. Above room temperature, two phase transitions were observed at 398 K and 538 K. The C_3H_7 and NH_3 in $(C_3H_7NH_3)$ were separated in the ^1H MAS NMR spectra, and the CH_3, CH_2, and CH_2 units in $CH_3CH_2CH_2NH_3^+$ were clearly distinguished in the ^{13}C CP/MAS NMR spectra. The chemical shifts of ^1H, ^{13}C, and ^{14}N signals were constant at all temperatures, whereas those of ^{113}Cd decreased upon increasing the temperature. From these results, it is evident that the crystal geometries surrounding ^1H, ^{13}C, and ^{14}N do not change with temperature, whereas that surrounding ^{113}Cd does. Further information about the dynamics of this crystal can be derived from the $T_{1\rho}$ values of ^1H and ^{13}C, and the results show that these atoms have higher mobility at high temperatures. The ^{13}C $T_{1\rho}$ in CH_3 increased with temperature, and the same trend was observed in alkyl chains attached to the $(C_3H_7NH_3)$ cation due to a greater mobility toward the free end. In addition, the T_1 value of ^{113}Cd was obtained, and it was very active at high temperatures. Overall, the cationic motion is associated with fluctuation of the uniaxial rotation and becomes more excited with increasing temperature. The dynamics of ^{113}Cd ions in Cd–Cl bonds of $CdCl_6$ octahedra were strongly activated at higher temperatures, and these results are consistent with the rotational disorder of the $CdCl_4$ planes found by X-ray diffraction [22].

Author Contributions: A.R.L. interpreted the TGA, DSC, and NMR measurements, and designed the research and wrote the manuscript. S.H.K. performed the NMR experiments.

Conflicts of Interest: The authors declare no conflicts of interest.

References

1. Xu, C.Q.; Kondo, T.; Sakakura, H.; Kumata, K.; Takahashi, Y.; Ito, R. Optical third-harmonic generation in layered perovskite-type material $(C_{10}H_{21}NH_3)_2PbI_4$. *Solid State Commun.* **1991**, *79*, 245–248. [CrossRef]
2. Papavassiliou, G.C. Three-and low-dimensional inorganic semiconductors. *Prog. Solid State Ch.* **1997**, *25*, 125–270. [CrossRef]
3. Mitzi, D.B. A layered solution crystal growth technique and the crystal structure of $(C_6H_5C_2H_4NH_3)_2PbCl_4$. *J. Solid State Chem.* **1999**, *145*, 694–704. [CrossRef]

4. Zhou, H.C.; Long, J.R.; Yaghi, O.M. Introduction to metal-organic frameworks. *Chem. Rev.* **2012**, *112*, 673–674. [CrossRef] [PubMed]

5. Strank, S.D.; Eperon, G.E.; Grancini, G.; Menelaou, C.; Alcocer, M.J.P.; Leijtens, T.; Herz, L.M.; Petrozza, A.; Snaith, H.J. Electron-hole diffusion lengths exceeding 1 micrometer in an organometal trihalide perovskite absorber. *Science* **2013**, *342*, 341–344. [CrossRef] [PubMed]

6. Xing, G.C.; Mathews, N.; Sun, S.Y.; Lim, S.S.; Lam, Y.M.; Gratzel, M.; Mhaisalkar, S.; Sum, T.C. Long-range balanced electron- and hole-transport lengths in organic-inorganic $CH_3NH_3PbI_3$. *Science* **2013**, *342*, 344–347. [CrossRef] [PubMed]

7. Elseman, A.M.; Shalan, A.E.; Sajid, S.; Rashad, M.M.; Hassan, A.M.; Li, M. Copper-substituted lead perovskite materials constructed with different halides for working $(CH_3NH_3)_2CuX_4$-based perovskite solar cells from experimental and theoretical view. *ACS Appl. Mater. Inter.* **2018**, *10*, 11699–11707. [CrossRef] [PubMed]

8. Aramburu, J.A.; Garcia-Fernandez, P.; Mathiesen, N.R.; Garcia-Lastra, J.M.; Moreno, M. Changing the usual interpretation of the structure and ground state of Cu^{2+} layered perovskite. *J. Phys. Chem. C* **2018**, *122*, 5071–5082. [CrossRef]

9. De Jongh, L.J.; Botterman, A.C.; de Boer, F.R.; Miedema, A.R. Transition temperature of the two-dimensional Heisenberg ferromagnet with s = 1/2. *J. Appl. Phys.* **1969**, *40*, 1363–1365. [CrossRef]

10. Petersson, E.R.; Willett, R.D. Crystal structure of $(CH_3CH_2CH_2NH_3)_2MnCl_4$. *J. Chem. Phys.* **1972**, *56*, 1879–1882. [CrossRef]

11. Arend, H.; Hofmann, R.; Waldner, F. New phase transition in $(C_nH_{2n+1}NH_3)_2MnCl_4$. *Solid State Commun.* **1973**, *13*, 1629–1632. [CrossRef]

12. Yamazaki, H. Interlayer exchange field in $(C_nH_{2n+1}NH_3)_2CuCl_4$ with n = 1−6 and $(C_6H_5C_mH_{2m}NH_3)_2 CuCl_4$ with m = 1, 2 determind by parallel pumping experiment. *J. Phys. Soc. Jpn.* **1976**, *41*, 1911–1917. [CrossRef]

13. Jahn, I.R.; Knorr, K.; Ihringer, J. The Jahn-Teller effect and orientational order in $(C_nH_{2n+1}NH_3)_2 CuCl_4$, n = 1,2,3. *J. Phys. Condens. Matt.* **1989**, *1*, 6005–6018. [CrossRef]

14. Lucken, A.; Hagemann, H.; Bill, H. Raman study of the incommensurate layer crystal $(CH_3CH_2CH_2NH_3)_2MnCl_4$ (=PAMnC) from 10 to 300 K. *J. Phys. Condens. Matt.* **1991**, *3*, 5085–5098. [CrossRef]

15. Narita, N.; Yamada, I. Nonlinear magnetic-susceptibility of two-dimensional magnets $(C_nH_{2n+1}NH_3)_2CuCl_4$ with n = 1, 2 and 3. *J. Phys. Soc. Jpn.* **1996**, *65*, 4054–4061. [CrossRef]

16. Manaka, H.; Yamada, I.; Goto, T. Disappearance of the weak ferromagnetic moment under high pressure observed in the two-dimensional antiferromagnet $(C_3H_7NH_3)_2CuCl_4$ through magnetic susceptibility measurements. *J. Phys. Soc. Jpn.* **2002**, *71*, 2822–2823. [CrossRef]

17. Suzuki, K.-I.; Fujimori, H.; Asaji, T.; Ishimaru, S.; Ikeda, R.Z. ^1H, ^2H and ^{13}C NMR studies of cation dynamics in a layered perovskite-type incommensurate compound $(n-C_3H_7NH_3)_2CdCl_4$. *Naturforsch* **1976**, *57*, 451. [CrossRef]

18. Levstik, A.; Filipic, C.; Blinc, R.; Arend, H.; Kind, R. Dielectric properties of $(C_nH_{2n+1}NH_3)_2CdCl_4$ and $(NH_3(CH_2)_nNH_3)CdCl_4$ perovskite layer compounds. *Solid State Commun.* **1976**, *20*, 127–130. [CrossRef]

19. Ecolivet, C.; Kusto, W. Brillouin scattering in $(C_3H_7NH_3)_2CdCl_4$. *Ferroelectrics* **1990**, *105*, 285–290. [CrossRef]

20. Kusto, W.J.; Rivera, J.-P.; Schmid, H. Birfringence of low-temperature phases of ferroelastic bis(n-propylammonium) tetrachlorocadmate. *Ferroelectrics* **1992**, *15*, 191–196. [CrossRef]

21. Chapuis, G. Study of the first-order phase transition of $(C_3H_7NH_3)_2CdCl_4$ at 183K by X-ray diffraction of the two phases. *Acta Cryst. B* **1978**, *34*, 1506–1512. [CrossRef]

22. Doudin, B.; Chapuis, G. Study of the modulated phase of $(C_3H_7NH_3)_2CdCl_4$ by single-crystal X-ray diffraction. *Acta Cryst. B* **1988**, *44*, 495–502. [CrossRef]

23. Yoshinari, T.; Matsuyama, T.; Achiwa, N.; Yamaoka, H.; Aoyagi, K. ESR and optical studies on $Cl_2{}^-$ in single crystals of $(C_nH_{2n+1}NH_3)_2CdCl_4$ with n = 1,2 and 3. *J. Phys. Soc. Jpn.* **1987**, *56*, 3354–3361. [CrossRef]

24. Blinc, R.; Burgar, M.; Lozar, B.; Seliger, J.; Slak, J.; Rutar, V.; Arend, H.; Kind, R. Proton NMR study of the structural phase transition in perovskite layer compounds: $(C_nH_{2n+1}NH_3)_2CdCl_4$ and $(NH_3-(CH_2)_n-NH_3)CdCl_4$. *J. Chem. Phys.* **1977**, *66*, 278–287. [CrossRef]

25. Koenig, J.L. *Spectroscopy of Polymers*; Elsevier: New York, NY, USA, 1999.

26. White, M.A.; Granville, N.W.; Davies, N.J.; Staveley, L.A.K. The heat capacity of the layer compounds $(CH_3CH_2CH_2NH_3)_2MnCl_4$ and $(CH_3CH_2CH_2NH_3)_2CdCl_4$ from 10 K to 300 K. *J. Phys. Chem. Solids* **1981**, *42*, 953–965. [CrossRef]

27. Lim, A.R. Behavior of H_2O surrounding NH_4^+ and Al^{3+} in $NH_4Al(SO_4)_2 \cdot 12H_2O$ by ^{1}H MAS NMR, ^{14}N NMR, and ^{27}Al NMR. *RSC Adv.* **2017**, *7*, 55276–55281. [CrossRef]

28. Mcbrierty, V.J.; Packer, K.J. *Nuclear Magnetic Resonance in Solid Polymers*; Cambridge University Press: Cambridge, UK, 1993.

29. Sakida, S.; Kawamoto, Y. [113]Cd MAS and static NMR study of halogenocadmate crystals. *J. Phys. Chem. Solids* **2002**, *63*, 151–161. [CrossRef]

30. Abragam, A. *The Principles of Nuclear Magnetism*; Oxford University Press: Oxford, UK, 1961.

31. Abrahams, S.C. Ferroelasticity [ferroelectrics, magnetics and superconductors]. *Mater. Res. Bull.* **1971**, *6*, 881–890. [CrossRef]

32. Salje, E.K.H. *Phase Transitions in Ferroelastic and Co-Elastic Crystals*; Cambridge University Press: Cambridge, UK, 1990.

33. Aizu, K. Determination of the state parameters and formulation of spontaneous strain for ferroelastics. *J. Phys. Soc. Jpn.* **1970**, *28*, 706–716. [CrossRef]

34. Sapriel, J. Domain-wall orientations in ferroelastics. *Phys. Rev. B* **1975**, *12*, 5128–5140. [CrossRef]